A HYBRID METHOD FOR UNCERTAINTY PROPAGATION OF ORBITAL MOTION AROUND THE EARTH

Inkwan Park[(1)] **and Daniel J. Scheeres**[(2)]

[(1)]*University of Colorado at Boulder, 429 UCB, Boulder, CO, 80309, U.S.A.,*
inkwan.park@gmail.com
[(2)]*University of Colorado at Boulder, 429 UCB, Boulder, CO, 80309,*
U.S.A.,scheeres@colorado.edu

Abstract: *In this paper, we present a new analytical nonlinear uncertainty propagation method that improves computational efficiency while maintaining accuracy. The salient idea of the suggested method, called a hybrid method, is a combination of the advantages of a simplified dynamical system (SDS) and state transition tensor (STT). The SDS, higher-order averaged dynamics, propagates a given state more efficiently by reducing the nonlinearity of a full dynamical system, and the STT directly maps a given uncertainty to any desired epoch. In this research, we apply the hybrid method for the non-Keplerian motion including multiple perturbations and verify the accuracy and the improvement of the computational efficiency. As a result, this research shows that the hybrid method is applicable to map uncertainty accurately, as well as provides even higher efficiency, approximate 0.002% processing time required, than the Monte-Carlo simulation with the SDS itself.*

Keywords: *simplified dynamical system, orbit uncertainty, semi-analytic solution, state transition tensor, perturbation theory*

1. Introduction

Space situational awareness (SSA) of Earth-orbiting particles has become increasingly important for the protection of current space properties and for guaranteeing the safety of future missions as the number of Resident Space Objects (RSOs) rapidly grows. For that reason, a technique for the propagation of state uncertainty consistent with the highly nonlinear dynamical environment[1, 2] becomes one of the most significant topics in the SSA. This nonlinearity of the dynamics prevents a traditional linearized mapping technique, such as the state transition matrix (STM)[3], from satisfying a required accuracy. In Junkins et al.[1], it is demonstrated that a fundamental assumption of the linearized mapping technique, Gaussianity, is no longer valid: an Earth-orbiting object in the Cartesian space does not preserve normality when propagated over time. Thus, various methods (e.g., Monte-Carlo sampling with high-fidelity simulation[4], polynomial chaos expansions[5], and Gaussian mixture models[6, 7, 8, 9]) have been proposed to incorporate the nonlinear effects in an orbiting motion and to represent the non-Gaussianity of the resulting probability distribution.

The purpose of this research is to apply a new method, called a hybrid method[10], to the non-Keplerian problem and to verify the accuracy and the computational efficiency of the method statistically. The hybrid method[10], in short, combines advantages of a simplified dynamical system (SDS)[11] and a state transition tensor (STT)[2, 12]. The SDS, based on higher-order averaged dynamics, was proposed and verified as a way to improve efficiency without losing accuracy[13]. The STT expands the STM to capture the nonlinear effects of the dynamics[2]. The advantage of the STT is to express a distribution at any arbitrary epoch as a function of a nominal trajectory and an

initial deviation. We apply the hybrid method to the non-Keplerian problem including multiple per-turbations: the earth oblateness, a direct solar radiation pressure (SRP), and gravitational attractions due to the Sun and moon (lunisolar effect). Then, the accuracy of the propagated uncertainty and the improvement of computational efficiency are investigated statistically. The SDS is derived from a Lie transformation defined by Deprit[14] up to the second-order; and the STT is considered up to the second-order. Ephemerides of the Sun and the moon are calculated from the JPL ephemeris file (DE405) from January 19, 2008 00:00:00 UCT to February 2, 2008, 23:59:59 UCT (15 days).

In Section 2, an overview of the SDS[11, 13], the STT[2, 12], and a procedure for combining the advantages are described. Then, two statistical approaches for verifying the accuracy of the method, comparison of the moments of PDFs and statistical energy test[15, 16], are addressed in Section 3. We test the hybrid method through two simulations in Section 4. In order to magnify the effects due to SRP and lunisolar attraction, high altitude cases, medium earth orbit (MEO) and highly eccentric orbit (Molniya) are chosen as examples. A numerical integration of 30,000 samples with a full dynamics, i.e., Monte-Carlo simulation, is assumed as the truth. We verify the accuracy of the propagated uncertainty with the hybrid method through the statistical methods. Then, we quantify the improvement of computational efficiency with elapse time for each process: Monte-Carlo simulations with the full dynamics and with the SDS[13], and the hybrid method. Throughout this research, the hybrid method is verified to successfully propagate the uncertainty under the multiple perturbations. In addition, it has even lower computational burden: the elapse time is less than 0.002% of the Monte-Carlo simulation with the full dynamics, approximately.

2. The Hybrid Method

The theoretical framework of the hybrid method consists of two parts: SDS and STT. In this section, we briefly review each idea and describe a procedure for combining the two ideas.

2.1. Simplified Dynamical System

In previous research[13, 11], we have proposed a simplified dynamical system (SDS) for improving a computational efficiency and investigating a dominant variation in mapping uncertainty. A primary idea of the SDS is reducing the nonlinearity of the full dynamical system by eliminating the short-period terms as seen in Eq. (1).

$$\mathbf{x} = \mathbf{x}_0 + \mathbf{x}_s + \mathbf{x}_{sp} + \mathbf{x}_{lp} \tag{1a}$$

$$\overline{\mathbf{x}} = \mathbf{x}_0 + \mathbf{x}_s + \overline{\mathbf{x}_{sp}} + \mathbf{x}_{lp}, \tag{1b}$$

where $\mathbf{x}_0$, $\mathbf{x}_s$, $\mathbf{x}_{sp}$, $\mathbf{x}_{lp}$, and $\overline{\mathbf{x}_{sp}}$ represent an initial condition, the secular, short-period, long-period variations, and an averaged short-period variation, respectively. Thus, conceptually, the SDS is an averaged dynamical system, such as the averaged Lagrange Planetary Equations (LPEs) [17]. The SDS, however, includes the higher-order averaged solutions for secular and long-period variations.

The higher-order averaged dynamics is obtained by a canonical transformation method. We introduce a Lie transformation proposed by Deprit[14]. The Deprit-Lie transformation (DL-

transformation) provides a systematic way to transform a given Hamiltonian,

$$\mathcal{H}(x,X;\varepsilon) = \sum_{n \geq 0} \frac{\varepsilon^n}{n!} \mathcal{H}_n(x,X), \tag{2}$$

onto an averaged Hamiltonian, Eq. (3), up to the required order.

$$\mathcal{K}(y,Y;\varepsilon) = \sum_{n \geq 0} \frac{\varepsilon^n}{n!} \mathcal{K}_n(y,Y) \tag{3}$$

After transforming the Hamiltonian, the SDS is defined based on the Hamiltonian equations in Eq. (4).

$$\frac{dy_i}{dt} = \frac{\partial \mathcal{K}}{\partial Y_i}, \quad \frac{dY_i}{dt} = -\frac{\partial \mathcal{K}}{\partial y_i}, \quad (i=1,\ldots,m) \tag{4}$$

where m represents a dimension of the generalized coordinates, y, and the conjugate moments, Y. Deprit[14] and Kamel[18] have discussed more details for applying the DL-transformation.

Proper Initial Condition for the SDS
Theoretically, the short-period variation becomes zero by averaging. However, in general, the averaged short-period variation, $\overline{x_{sp}}$, has a non-zero value, which depends on a given initial condition as follows:

$$\overline{x_{sp}} = \frac{1}{2\pi} \int_0^{2\pi} x_{sp} \, dl = \mathcal{C}, \quad \begin{cases} \mathcal{C} = 0 & \text{if } \{l|l = 0,\ 2\pi\} \\ \mathcal{C} \neq 0 & \text{Otherwise.} \end{cases} \tag{5}$$

This property plays an important role in applying the SDS because it is based on the mean orbit. The proper initial condition stands for the mean orbit at an initial epoch, which corresponds to a given initial condition in the osculating space. In this research, a numerical method, i.e., the initial offset correction[11], is applied to generate the proper initial condition.

2.2. State Transition Tensor

The STT directly maps an initial deviation to any epoch with respect to a nominal trajectory[2] and captures the nonlinearity of dynamics by including higher-order terms of a Taylor series expansion[2, 12]. In this research, we focus on these advantages of the STT for accurate and more efficient propagation of uncertainty.

A state at an arbitrary epoch, t, can be expressed as

$$x(t) = \phi(t; x^0, t^0), \tag{6}$$

where ϕ represents the solution flow[2], which defines a state at any epoch as a function of the initial condition. x and x^0 denote states at an arbitrary epoch ($t = t$) and at the initial epoch ($t = 0$), i.e., $x^0 = x(t^0)$, respectively[2]. The equation of motion is a time derivative of the solution flow as follows:

$$\dot{x}(t) = f(t, x(t)), \tag{7a}$$

3

where $\boldsymbol{f}$ denotes the dynamics[2, 12]. A deviation at an arbitrary epoch can be expressed as a function of the initial condition through the solution flow as

$$\delta\boldsymbol{x}(t) = \phi(t;\boldsymbol{x}^0+\delta\boldsymbol{x}^0,t^0) - \phi(t;\boldsymbol{x}^0,t^0) \tag{8a}$$

$$= \sum_{p=1}^{m} \frac{1}{p!} \Phi_{i,k_1...k_p} \delta\boldsymbol{x}_{k_1}^0 \ldots \delta\boldsymbol{x}_{k_p}^0. \tag{8b}$$

Simlilarly, the time derivative of the deviation can be rewritten, from Eq. (8a), as follows:

$$\delta\dot{\boldsymbol{x}}(t) = \boldsymbol{f}(t, \phi(t;\boldsymbol{x}^0+\delta\boldsymbol{x}^0,t^0)) - \boldsymbol{f}(t, \phi(t;\boldsymbol{x}^0,t^0)) \tag{9a}$$

$$= \sum_{p=1}^{m} \frac{1}{p!} A_{i,k_1...k_p} \delta\boldsymbol{x}_{k_1} \ldots \delta\boldsymbol{x}_{k_p}. \tag{9b}$$

Equations (8b) and (9b) are a form of a Taylor series expansion for each case: m and k_j are an order of expansion and the k_j-th component of the state vector($k_j \in \{1,2,\ldots,n\}$), respectively. $\Phi_{i,k_1...k_p}$ and $A_{i,k_1...k_p}$ represent the STT and a local dynamics tensor (LDT)[12], and they are defined as follows:

$$\Phi_{i,k_1...k_p} = \frac{\partial^p \boldsymbol{x}_i}{\partial \boldsymbol{x}_{k_1}^0 \ldots \partial \boldsymbol{x}_{k_p}^0}, \tag{10}$$

$$A_{i,k_1...k_p} = \frac{\partial^p \boldsymbol{f}_i}{\partial \boldsymbol{x}_{k_1} \ldots \partial \boldsymbol{x}_{k_p}}\bigg|_{\boldsymbol{x}=\boldsymbol{x}^*}. \tag{11}$$

The STT becomes a traditional state transition matrix (STM) where $m = 1$. The LDT is evaluated along the nominal trajectory $\boldsymbol{x}^*$. As discussed in Park et al.[2], time derivatives of the STT are defined as a function of the LDT and STT; for instance, the differential equation of the second-order STT is given below.

$$\dot{\Phi}^{i,ab} = A^{i,\alpha}\Phi^{\alpha,ab} + A^{i,\alpha\beta}\Phi^{\alpha,a}\Phi^{\beta,b} \tag{12}$$

2.3. Combination of the SDS and STT

As demonstrated in Park et al.[10], the advantages of the SDS and STT are combined to propagate uncertainty accurately and to improve the computational efficiency. The hybrid method combines the advantages through the two steps given below:
  (1) Deriving the SDS through the DL-transformation and computing the proper initial conditions.
  (2) Replacing the equations of motion, Eq. (7a), through the DL-transformation with the SDS in defining the LDT with Eq. (11), and then calculating the STT up to the desired order by integrating Eq. (12).

Therefore, the combination makes it possible to map any given initial uncertainty directly to any epoch by Eq. (8b) without applying the Monte-Carlo simulation.

3. Statistical Verification Methods

3.1. Comparing the Moments of PDFs

We compare the moments of PDF up to fourth-order. Since the first four moments quantify the non-Gaussianity of a distribution, one can intuitively see if the propagated distribution and of the truth coincide. The mean and variance from the distribution are used as the first two moments. For the third and fourth order moments, the standardized moment is introduced, which are known as the skewness and kurtosis, respectively. The standardized moment, $\overline{\mu}_k$, can be calculated from Eq. (13),

$$\overline{\mu}_k = \frac{\mu_k}{\mu_2^{k/2}}, \tag{13}$$

where μ_k represents the central moments[19]. The skewness and kurtosis are exactly defined when $k = 3$ and $k = 4$, respectively.

3.2. Statistical Energy Test

For more rigorous verification, the statistical energy test is introduced instead of using traditional tests, such as Kolmogorov-Smirnov test or Pearson's chi-squared test, to measure the Goodness-of-Fit (GoF) for testing the hypothesis. The energy test is computationally more expensive than the traditional tests, but it is an optimized method to compare multivariate PDFs[15, 16]. Since uncertainties discussed in this research are defined in six-dimensional space, we introduce the energy test for the verification.

The statistical energy test assumes that a relationship between statistical observations is similar to the notion of potential energy[20]. A test statistic (ϕ_{NM}) is defined in Eq. (14), and it becomes the minimum if the two distributions coincide[15].

$$\phi_{\text{NM}} = \frac{1}{N^2} \sum_{j>i} R(|\boldsymbol{x}_i - \boldsymbol{x}_j|) - \frac{1}{NM} \sum_i \sum_j R(|\boldsymbol{x}_i - \boldsymbol{y}_j|), \tag{14}$$

where $\boldsymbol{x}_i$ and $\boldsymbol{y}_j$ represent the i-th observation and j-th model sample vectors, respectively. The logarithmic distance function, R, is used[10, 13]. N and M are the number of observations and model samples. The hypothesis test is designed by replacing the observations with a PDF from the true distribution and the model samples with a PDF from the distribution propagated with the hybrid method.

In this research, the null and alternate hypotheses are

$$\begin{aligned} H_0 &: \mathfrak{U}_{\text{truth}}(\boldsymbol{x}) = \mathfrak{U}_{\text{hybrid}}(\boldsymbol{x}), \\ H_1 &: \mathfrak{U}_{\text{truth}}(\boldsymbol{x}) \neq \mathfrak{U}_{\text{hybrid}}(\boldsymbol{x}), \end{aligned} \tag{15}$$

where $\mathfrak{U}$ represents the PDF of propagated uncertainty. A significance level α is assumed as 5%, and the p-value is obtained from the statistical energy test. By definition of the hypothesis test, if the null hypothesis is accepted, i.e., the propagated uncertainty with the hybrid method is compatible to the truth, we can conclude that the hybrid method propagates the uncertainty accurately with a $(1 - \alpha)$ confidence level.

4. Hamiltonian Dynamics for Non-Keplerian Motion

We consider perturbations due to the earth oblateness, a direct solar radiation pressure, and gravitational attractions due to massive bodies (e.g., the moon and the Sun.) The mean motion of the moon is used as the small parameter (i.e., $\varepsilon = n_2$) to group the Hamiltonian in expandable form as

$$\mathcal{H} = \sum_{n=0}^{4} \frac{\varepsilon^n}{n!} \mathcal{H}_n. \tag{16}$$

Each Hamiltonian in Eq. (16) corresponds to the perturbing terms included in the non-Keplerian motion as given below.

$$
\begin{aligned}
\mathcal{H}_0 &= \mathcal{H}_k = -\frac{\mu}{2a}, \\
\mathcal{H}_1 &= \mathcal{H}_\odot, \\
\mathcal{H}_2 &= \mathcal{H}_o + \mathcal{H}_{3b,\odot 1} + \mathcal{H}_{3b,\odot} + \mathcal{H}_\odot, \\
\mathcal{H}_3 &= 0, \\
\mathcal{H}_4 &= \mathcal{H}_s + \mathcal{H}_{3b,\odot 2},
\end{aligned}
\tag{17}
$$

where $\mathcal{H}_k$, $\mathcal{H}_o$, $\mathcal{H}_s$, and $\mathcal{H}_{3b,\odot}$ indicate the Hamiltonians for the Keplerian motion, earth oblateness, solar radiation pressure, and gravitational attraction due to the Sun. The others, $\mathcal{H}_{3b,\odot 1}$ and $\mathcal{H}_{3b,\odot 1}$, are gravitational attraction due to the moon including third-order expanded term of the Legendre polynomial. Lastly, $\mathcal{H}_\odot$ and $\mathcal{H}_\odot$ are conjugates of the extended variables for describing the motion of the Sun and moon [21, 22]. A detailed description about each Hamiltonian will be presented in this section.

4.1. Earth Oblateness

The potential due to the earth oblateness is

$$\mathcal{U}_o = \frac{\mu}{r_1} \sum_{n=2} J_n \left(\frac{\alpha}{r_1}\right)^n P_n(\sin \delta), \tag{18}$$

where μ, α, δ, and $P_n(x)$ denote the gravitational parameter of the Earth, earth radius, declination of the satellite, and the Legendre polynomial. By using an expression by Brouwer[23], $\sin \delta$ is defined in terms of the orbital elements.

$$\sin \delta = \sin i \sin(g + f)$$

Since this research considers the second order zonal harmonics, the Hamiltonian of the earth oblateness can be simply define as

$$\mathcal{H}_o = \frac{2!}{\varepsilon^2} \left[\frac{1}{2} \frac{\mu}{r_1} \left(\frac{\alpha}{r_1}\right)^2 J_2 \left[\frac{3}{2} s^2 - \frac{3}{2} s^2 \cos(2f + 2g) - 1 \right] \right]. \tag{19}$$
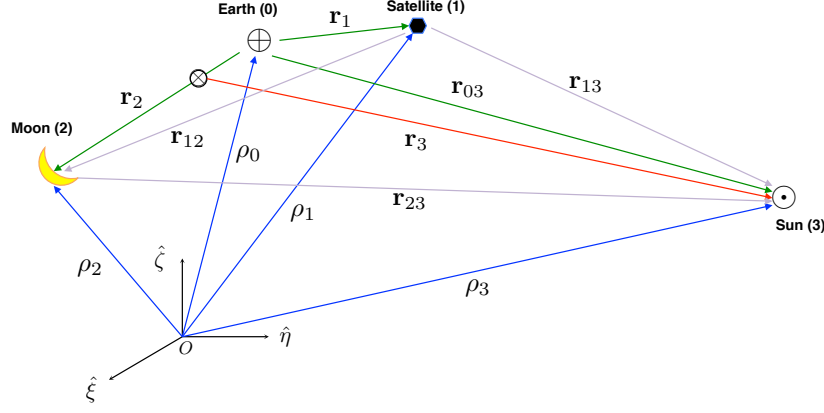
Figure 1. Relative positions of the Earth, satellite, moon, and Sun: the inertial coordinates frame is expressed in unit vectors $(\hat{\xi}, \hat{\eta}, \hat{\zeta})$ and a symbol $\otimes$ indicates the barycenter between the Earth and moon.

4.2. Gravitational Attraction due to the Sun and Moon

A spatial distribution is depicted in Fig. 1. A gravitational potential due to N objects is simply defined in Eq. (20) with the relative position vector[17].

$$\mathscr{U}_{3b} = \frac{1}{2} \sum_{i=0}^{N} \sum_{\substack{j=0 \\ j \neq i}}^{N} \frac{G m_i m_j}{|\boldsymbol{r}_{ij}|}, \tag{20}$$

where G, m_i, and $\boldsymbol{r}_{ij}$ represent the universal gravitational constant, mass of i-th body, and a relative position vector between i and j bodies, respectively. By assuming $r_1 \ll r_{03}$, Eq. (20) can be rewritten as follows[24]:

$$\mathscr{U}_{3b} = \frac{\mu_2 r_1^2}{2 r_2^3} (3 \cos^2 \theta_{12} - 1) + \frac{\mu_3 r_1^2}{2 r_3^3} (3 \cos^2 \theta_{13} - 1) + \frac{\mu_2 r_1^3}{2 r_2^4} (5 \cos^3 \theta_{12} - 3 \cos \theta_{12}), \tag{21}$$

where μ_2 and μ_3 represent the gravitational parameters of the moon and the Sun, respectively.[1] An angular distance θ_{1m} can be obtained from

$$\cos \theta_{1m} = \frac{\boldsymbol{r}_1 \cdot \boldsymbol{r}_m}{r_1 r_m} = \hat{\boldsymbol{r}}_1 \cdot \hat{\boldsymbol{r}}_m. \tag{22}$$

The angular distance θ_{1m} is the included angle between the position vectors of the satellite and m-th perturbing body. The next step is to express Eq. (22) in terms of the orbital elements. This step is carried out based on Fig. 2, and the position vectors is rewritten in Eq. (23) ($u_\star = f_\star + g_\star$).

$$\hat{\boldsymbol{r}}_1 = \begin{pmatrix} \cos h_1 \cos(f_1 + g_1) - \cos i_1 \sin h_1 \sin(f_1 + g_1) \\ \cos i_1 \cos h_1 \sin(f_1 + g_1) + \sin h_1 \cos(f_1 + g_1) \\ \sin i_1 \sin(f_1 + g_1) \end{pmatrix}$$

$$\hat{\boldsymbol{r}}_\star = \begin{pmatrix} \cos h_\star \cos u_\star - \cos i_\star \sin h_\star \sin u_\star \\ \cos i_\star \cos h_\star \sin u_\star + \sin h_\star \cos u_\star \\ \sin i_\star \sin u_\star \end{pmatrix} \tag{23}$$

---

[1] A more detailed procedure for rewriting Eq. (20) to (21) can be found in [17].

7
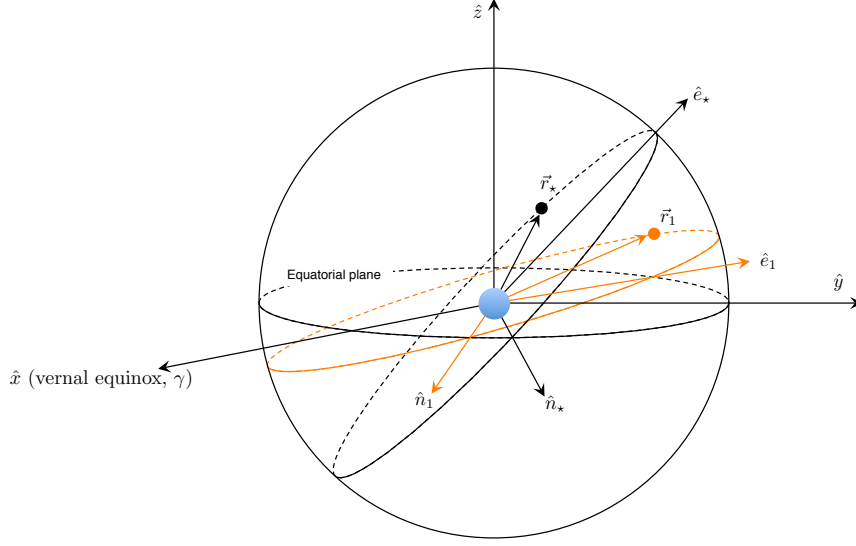
Figure 2. Geometric relation between two orbiting bodies with respect to a central body: direction cosines for defining the potential due to perturbing bodies and solar radiation pressure are derived from this geometry.

By substituting Eq. (23) into (22), one can get

$$\cos\theta_{1\star} = T_{c,\star}\cos f_1 + T_{s,\star}\sin f_1, \tag{24}$$

where

$$
\begin{aligned}
T_{c,\star} = \frac{1}{4}\{&(c_1+1)(c_\star+1)\cos(g+h-h_\star-u_\star) + (c_1-1)(c_\star-1)\cos(g-h+h_\star-u_\star) \\
&-(c_1+1)(c_\star-1)\cos(g+h-h_\star+u_\star) - (c_1-1)(c_\star+1)\cos(g-h+h_\star+u_\star)\} + s\,s_\star\sin g\sin(u_\star) \\
T_{s,\star} = \frac{1}{4}\{&(c_1-1)(c_\star+1)\sin(g-h+h_\star+u_\star) - (c_1+1)(c_\star+1)\sin(g+h-h_\star-u_\star) \\
&-(c_1-1)(c_\star-1)\sin(g-h+h_\star-u_\star) + (c_1+1)(c_\star-1)\sin(g+h-h_\star+u_\star)\} + s\,s_\star\cos g\sin(u_\star).
\end{aligned}
$$

As a result, the gravitational potential is

$$
\begin{aligned}
\mathscr{U}_{3b} =& \frac{\mu_2 r_1^2}{2r_2^3}\{3(T_{c,2}\cos f_1 + T_{s,2}\sin f_1)^2 - 1\} + \frac{\mu_3 r_1^2}{2r_3^3}\{3(T_{c,3}\cos f_1 + T_{s,3}\sin f_1)^2 - 1\} \\
&+ \frac{\mu_2 r_1^3}{2r_2^4}\left\{5(T_{c,2}\cos f_1 + T_{s,2}\sin f_1)^3 - 3(T_{c,2}\cos f_1 + T_{s,2}\sin f_1)\right\},
\end{aligned} \tag{25}
$$

and the Hamiltonians are given below.

$$
\begin{aligned}
\mathscr{H}_{3b,\odot} &= \frac{2!}{\varepsilon^2}\left[\frac{\mu_3 r_1^2}{2r_3^3}\{3(T_{c,3}\cos f_1 + T_{s,3}\sin f_1)^2 - 1\}\right], \\
\mathscr{H}_{3b,\odot 1} &= \frac{2!}{\varepsilon^2}\left[\frac{\mu_2 r_1^2}{2r_2^3}\{3(T_{c,2}\cos f_1 + T_{s,2}\sin f_1)^2 - 1\}\right], \\
\mathscr{H}_{3b,\odot 2} &= \frac{2!}{\varepsilon^2}\left[\frac{\mu_2 r_1^3}{2r_2^4}\left\{5(T_{c,2}\cos f_1 + T_{s,2}\sin f_1)^3 - 3(T_{c,2}\cos f_1 + T_{s,2}\sin f_1)\right\}\right].
\end{aligned} \tag{26}
$$

8

4.3. Solar Radiation Pressure

The Hamiltonian for the SRP is[21]

$$\mathcal{H}_s = -\beta \frac{r}{r_{\odot,sat}^2} \cos\theta_{13}, \tag{27}$$

where

$$\beta = (1+\rho)\frac{A_{sat}}{m_{sat}}P_\Phi.$$

β represents the solar perturbation strength. The solar constant, P_Φ, is approximately $1 \times 10^8\, kg\,km^3/s^2/m^2$ [24]. We assume that the reflectivity (ρ) and area-to-mass ratio (A_{sat}/m_{sat}) are 0.2 and 2.0 m^2/kg, respectively. From Eq. (24), the Hamiltonian becomes

$$\mathcal{H}_s = \frac{4!}{\varepsilon^4}\left[-\beta\frac{r_1}{r_{13}^2}\left(T_{c,3}\cos f_1 + T_{s,3}\sin f_1\right)\right]. \tag{28}$$

5. Simulations

The hybrid method is tested with two scenarios: a Medium-Earth-Orbit (MEO) and a highly elliptical orbit (Molniya). These cases demonstrate the capabilities of the proposed method when propagating the state uncertainty, including the multiple perturbations discussed above. The initial conditions are chosen to avoid singularity problems, e.g., zero eccentricity, zero inclination, and critical inclination, because the current hybrid method is defined in terms of the Delaunay variables. Table 1 presents the initial orbit conditions for each case. The ephemerides of the Sun and moon have been obtained from the JPL ephemeris file (DE405) from January 19, 2008 00:00:00 UCT to February 2, 2008, 23:59:59 UCT (15 days), which covers the period studied. For the Monte Carlo

Table 1. Initial Keplerian elements for RSOs on MEO and Molniya orbit

	MEO	Molniya
Semimajor axis, a, (km)	26578.14	26578.14
Eccentricity, e	0.01	0.74
Inclination, i, (deg)	55	63
Longitude of the ascending node, Ω, (deg)	45	45
Argument of periapsis, ω, (deg)	60	270
Mean anomaly, l, (deg)	105	105

simulation, normally distributed 30,000 samples within a specified 3-σ region are generated with respect to the given initial condition. A Gaussian error (1-σ) is assumed with standard deviations of 10 km in the semi-major axis, 0.05 in eccentricity, and 0.01° in the inclination, longitude of ascending node, the argument of the pericenter, and the mean anomaly directions. The samples are propagated for 30-orbital periods ($\approx$ 15 days.) A propagated uncertainty from the Monte-Carlo simulation with the full dynamics is assumed as the truth. The *ode45* function in MATLAB is used as a numerical integrator. In this section, we verify the accuracy of the hybrid method through two statistical methods. Then, we compare an elapse time of the hybrid method to those from the Monte-Carlo simulation with the full dynamics and with the SDS itself to show the improvement of computational efficiency.

9

5.1. Result I: Verification of the Accuracy

5.1.1. Uncertainty for Highly Elliptical Orbit Objects from the Hybrid Method

Comparing the Moments of PDFs
 The hybrid method maps uncertainty in the Delaunay variables space. For the verification, we project the result onto the Cartesian coordinate space since general applications for SSA, such as collision assessment, are considered on that space. Figs. 3 and 4 are the propagated uncertainties from the hybrid method and the truth, plotted on the δx-$\delta \dot{x}$ phase-space. Both figures present the histogram of the conditional PDF on the $\delta \dot{x}$(ER/s) axis (top-left), that on δx(ER) axis (bottom-right), and the distributions of the samples on the δx-$\delta \dot{x}$ phase space (top-right). The histograms show that the Gaussianity is no longer maintained due to the nonlinear effects of the dynamics; the distributions on each figure present that both results are well matched.[2] For the sake of verifying
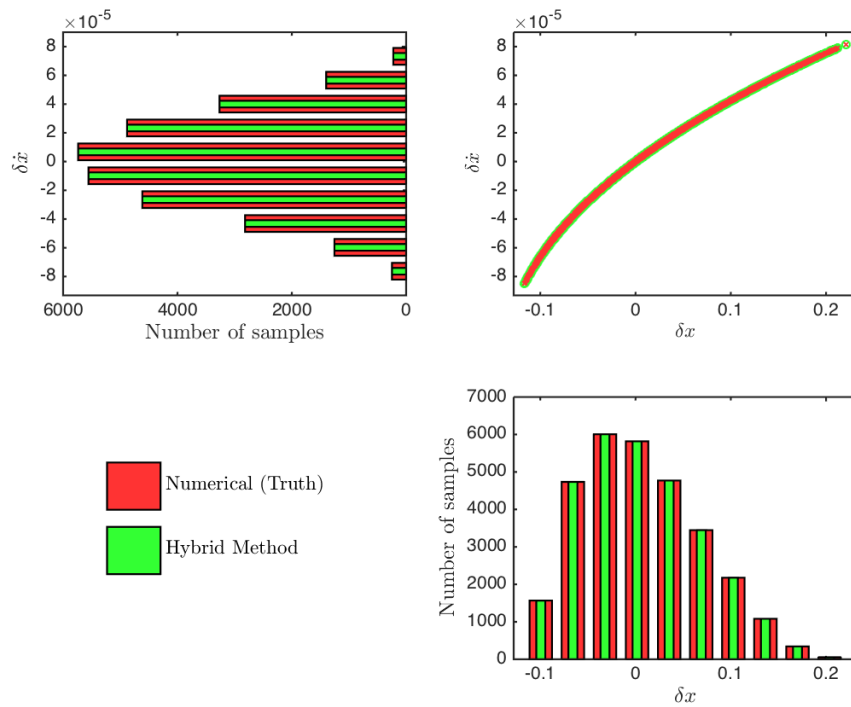
Figure 3. Sample point distribution and its conditional histograms after 30 orbit periods of propagation in MEO.

the results, Table 2 quantifies the moments of the distributions and the relative errors with respect to the truth up to fourth-order. In order to show the accuracy of the higher-order STT, we test the hybrid method with the first-order STT (i.e., STM) and with the the second-order STT. On the table, the first row summarizes the moments and the relative errors for the MEO case, and the second row for the Molniya case. All values are normalized with respect to earth radius (ER). The table shows that the relative errors on *x*-axis are less than 0.2% from the truth except the skewness for the

---

[2]The distributions on the different phase-spaces are similar, we do not include the results on those spaces.
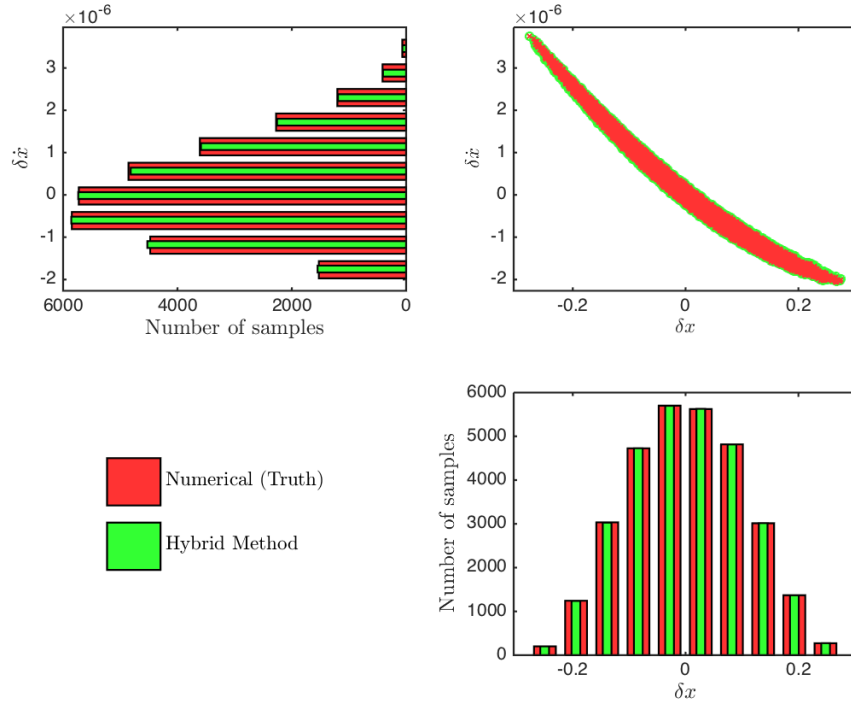
Figure 4. Sample point distribution and its conditional histograms after 30 orbit periods of propagation in Molniya.

Molniya case. In addition, it is also possible to see that the hybrid method with the higher-order STT propagates uncertainty more accurately.

Table 2. Central moments and relative errors on *x*-axis after 30-orbital periods of propagation (top: MEO, bottom: Molniya)

	Mean		Variance		Skewness		Kurtosis	
	μ_1	$\Delta\,(\%)$	μ_2	$\Delta\,(\%)$	$\overline{\mu}_3$	$\Delta\,(\%)$	$\overline{\mu}_4$	$\Delta\,(\%)$
STM	6.5518e-3	8.3259e-3	3.8465e-3	4.6719e-2	4.4733e-1	2.4626e-1	2.5951	5.6909e-2
STT	6.5509e-3	2.1223e-3	3.8476e-3	1.7182e-2	4.4839e-1	1.1624e-2	2.5965	2.1037e-3
STM	7.1008e-4	1.7762e-1	1.0305e-2	2.3053e-1	1.7169e-2	2.8532	2.3937	5.5345e-4
STT	6.8703e-4	1.5280e-1	1.0304e-2	2.2914e-1	1.6206e-2	2.8202	2.3936	2.8641e-4

Statistical Energy Test

The statistical energy test is applied to both simulations for verifying the accuracy more rigorously. Fig. 5 shows the *p*-values at every five orbital periods. The significance level for the hypothesis test is set $\alpha = 5\%$. As seen in the figures, the obtained *p*-values are larger than the designated significance level; thus, we can conclude that the propagated uncertainty with the hybrid method describes the truth with a 95% confidence level.

(a) MEO case   (b) Molniya case
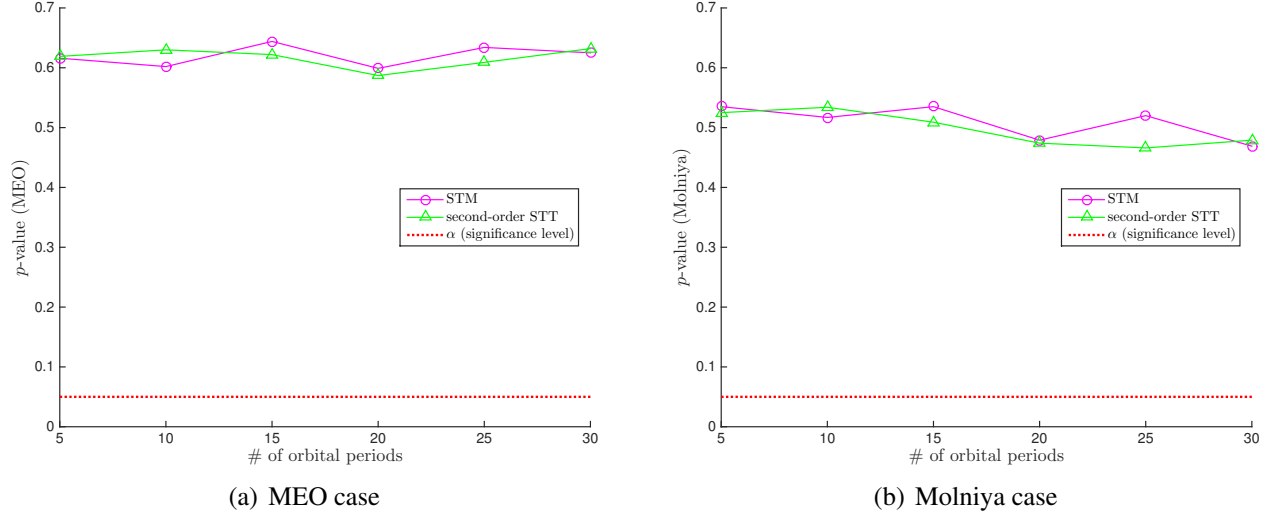
Figure 5. Time history of p-values vs. significance level (α=0.05)

5.2. Result II: Improvement in Computational Efficiency

The improvement in computational efficiency is investigated with the elapse time for uncertainty propagation. We compare the times obtained from three approaches: 1) Monte-Carlo simulation with the full dynamics, 2) Monte-Carlo simulation with the SDS, and 3) the hybrid method. All computations are performed on a laptop, 2.8 GHz Intel® Core i7 and 4 GB 1067 MHz DDR3. The elapse time is the average value acquired from 10 runs (the Monte-Carlo simulation with the full dynamics is run once.) The results are summarized in Table 3.

Table 3. Comparison of elapsed time in propagating the uncertainty (MEO)

Methodology	elapsed time (seconds)	Remarks
Numerical M-C	2.2782e6 ($\approx$ 26.4days)	—
SDS M-C	1.1279e5 ($\approx$ 1.3 days)	—
Hybrid method STT	51.3633	include elapsed time for computing the STT

As seen in the table, the hybrid method provides even higher performance in propagating the uncertainty than the others. There are 30,000 samples used in the Monte-Carlo simulations; thus, if one used more samples, the performance would have more dramatic difference.

6. Conclusion

In this research, we applied the hybrid method[10] to propagate uncertainty under multiple perturbations. The method uses the advantages of the simplified dynamical system and state transition tensor; thus, it provides more efficient way to map uncertainty. We compared the results from the hybrid method to those from the Monte-Carlo simulations based on the full dynamics (the truth) and the SDS. The verification of the accuracy and the improvement of efficiency are carried out through the statistical methods and the comparison of elapse times, respectively. For the given examples, the hybrid method maps uncertainty accurately at least up to fourth-order moment of

PDFs and 95% of the confidence level with only 0.002% of the elapse time of the Monte-Carlo simulation with the full dynamics. Therefore, we can conclude that the hybrid method propagates uncertainty accurately and efficiently under the given multiple perturbing environment.

7. References

[1] Junkins, J. L., Akella, M. R., and Alfriend, K. T. "Non-Gaussian Error Propagation in Orbital Mechanics." Journal of Astronautical Sciences, Vol. 44, No. 4, pp. 541–563, October-December 1996.

[2] Park, R. S. and Scheeres, D. J. "Nonlinear Mapping of Gaussian Statistics: Theory and Applications to Spacecraft Trajectory Design." Journal of Guidance, Control, and Dynamics, Vol. 29, No. 6, pp. 1367–1375, November-December 2006. doi:10.2514/1.20177.

[3] Tapley, B. D., Schutz, B. E., and Born, G. H. Statistical Orbit Determination. Elsevier Academic Press, Burlington, MA, 1 edn., 2004.

[4] Maybeck, P. S. Stochastic Models, Estimation and Control, Vol. 2. Academic Press, New York, NY, 1982.

[5] Jones, B. A., Doostan, A., and Born, G. H. "Nonlinear Propagation of Orbit Uncertainty Using Non-Intrusive Polynomial Chaos." Journal of Guidance, Control, and Dynamics, Vol. 36, No. 2, pp. 430–444, March-April 2013. doi:10.2514/1.57599.

[6] Horwood, J. T., Aragon, N. D., and Poore, A. B. "Gaussian Sum Filters for Space Surveillance: Theory and Simulations." Journal of Guidance, Control, and Dynamics, Vol. 34, No. 6, pp. 1839–1851, December 2011. doi:10.2514/1.53793.

[7] Terejanu, G., Singla, P., Singh, T., and Scott, P. D. "Uncertainty Propagation for Nonlinear Dynamic Systems Using Gaussian Mixture Models." Journal of Guidance, Control, and Dynamics, Vol. 31, No. 6, pp. 1623–1633, November-December 2008. doi:10.2514/1.36247.

[8] Giza, D., Singla, P., and Jah, M. "An approach for Nonlinear Uncertainty Propagation: Application to Orbital Mechanics." AIAA 2009-6082. AIAA, 2009.

[9] DeMars, K. J. Nonlinear Orbit Uncertainty Prediction and Rectification for Space Situational Awareness. thesis, University of Texas at Austin, December 2010.

[10] Park, I. and Scheeres, D. J. "The New Method for Nonlinear Propagation of Uncertainty for Non-Keplerian Motion (in preparation)." Journal of Guidance, Control, and Dynamics, 2015.

[11] Park, I., Scheeres, D. J., and Fujimoto, K. "The Effect of Dynamical Accuracy for Uncertainty Propagation." S. B. Broschart, J. D. Turner, K. C. Howell, and F. R. Hoots, editors, "Astrodynamics 2013," Vol. 150. August 2013.

[12] Fujimoto, K. and Scheeres, D. J. "Analytical Nonlinear Propagation of Uncertainty in the Two-Body Problem." Journal of Guidance, Control, and Dynamics, Vol. 35, No. 2, pp. 497–509, 2012. doi:10.2514/1.54385.

[13] Park, I. and Scheeres, D. J. "The Effect of Dynamical Accuracy for Uncertainty Propagation (accepted)." Journal of Guidance, Control, and Dynamics, 2015.

[14] Deprit, A. "Canonical Transformations Depending on a Small Parameter." Celestial Mechanics, Vol. 1, pp. 12–30, 1969.

[15] Aslan, B. and Zech, G. "Statistical energy as a tool for binning-free, multivariate goodness-of-fit tests, two-sample comparison and unfolding." Nuclear Instruments and Methods in Physics Research, Vol. 537, pp. 626–636, 2005. doi:10.1016/j.nima.2004.08.071.

[16] Aslan, B. The concept of energy in nonparametric statistics - Goodness-of-Fit problems and deconvolution. Ph.D. thesis, Universitat Siegen, 2004.

[17] Roy, A. E. Orbital Motion. Taylor and Francis Group, fourth edn., 2005.

[18] Kamel, A. A. "Perturbation Method in the Theory of Nonlinear Oscillations." Celestial Mechanics, Vol. 3, pp. 90–106, 1970.

[19] Grimmett, G. and Stirzaker, D. Probability and Random Processes. Oxford, England: Oxford University Press, 3rd edn., 2009. ISBN 978-0198572220.

[20] Szèkely, G. J. and Rizzo, M. L. "Energy Statistics: A Class of Statistics Based on Distances." Journal of Statistical Planning and Interference, Vol. 143, pp. 1249–1272, 2013. doi:10.1016/j.jspi.2013.03.018.

[21] Hori, G. I. "The effect of radiation pressure on the motion of an artificial satellite." J. B. Rosser, editor, "Space Mathematics Part 3," Vol. 7, pp. 167–182. American Mathematical Society, 1966.

[22] Saad, N. A., Khalil, K. I., and Amin, M. Y. "Analytical Solution for the Combined Solar Radiation Pressure and Luni-Solar Effects on the Orbits of High Altitude Satellites." The Open Astronomy Journal, Vol. 3, pp. 113–122, 2010.

[23] Brouwer, D. "Solution of the Problem of Artificial Satellite Theory without Drag." The Astronomical Journal, Vol. 64, No. 1274, pp. 378–396, 1959.

[24] Scheeres, D. J. Orbital Motion in Strongly Perturbed Environments. Springer, 2012.